Microscopic theory of the inverse spin galvanic effect in anisotropic Rashba models

Alessandro Veneri [1,2] Francesco Quintavalle [2,4] Thierry Valet [3] and Roberto Raimondi [2]

[1]*Dipartimento di Ingegneria dell'Informazione, Elettronica e Telecomunicazioni, Università La Sapienza, Via Eudossiana, 18, 00184 Roma, Italy*

[2]*Dipartimento di Matematica e Fisica, Università Roma Tre, Via della Vasca Navale 84, 00146 Roma, Italy*

[3]*MPhysX OÜ, Harju maakond, Tallinn, Lasnamäe linnaosa, Sepapaja tn 6, 15551, Estonia*

[4]*School of Science and Technology, Physics Division, Università di Camerino, Via Madonna delle Carceri, 62032 Camerino (MC), Italy*

(Received 5 December 2025; revised 29 January 2026; accepted 10 March 2026; published 27 March 2026)

The Rashba spin-orbit coupling (SOC) is a well-known mechanism for the spin-charge interconversion via the inverse and direct spin galvanic effects. The lack of a full inversion symmetry allows the coupling of the charge current and spin density. In this paper we investigate this phenomenon when the in-plane rotational symmetry is lowered to the C_{2v} and C_{3v} symmetry groups, whereby the electron spectrum becomes anisotropic. We find that in the C_{2v} case, depending on the ratio between the Rashba SOC strengths along the principal axes, the nonequilibrium spin density deviates notably from the 90° rotation, with respect to the applied electric field, which is familiar in the isotropic case. In the C_{3v} case, when a warping cubic in momentum term is present, whereas the standard 90° rotation of the spin density remains, the spin-charge interconversion depends on the intensity of the warping itself. The microscopic theory takes into account disorder including vertex corrections, via both the diagrammatic implementation of the Kubo formula and the quantum kinetic theory. We show that vertex corrections are crucial to capture the details of the inverse spin galvanic effect in contrast to previous treatments based on the constant broadening approximation.

DOI: 10.1103/b675-4wsd

I. INTRODUCTION

Spin-dependent phenomena in nonmagnetic materials lacking inversion symmetry have attracted a lot of attention in the last few decades, as these systems enable all-electrical control of the spin degree of freedom (DOF) without the need for external magnetic fields [1–6]. The underlying mechanisms arise from the relativistic spin-orbit coupling (SOC), which induces a spin-momentum locking that renders the spin and momentum DOFs fully interdependent [7–12]. Sources of SOC can manifest both uniformly and locally, with the former induced by the system's geometry and the associated crystalline potential [13,14] while the latter originates from randomly distributed fluctuations or proximity to adatom impurities [15–17].

Promising for the development of experimental spintronics devices [18], SOC landscapes enable charge-spin conversion phenomena that generate spin currents and densities. In particular, two effects, together with their Onsager reciprocal counterpart, have emerged as the most intriguing: the spin Hall effect (SHE) [19–23] and the inverse spin galvanic effect (ISGE), also frequently cited as the Edelstein effect (EE), whose denomination we will use from now on [24–30]. The former converts a charge current, driven by an external electric field, into a transverse spin current, while the latter converts an electric current into a nonequilibrium spin polarization. Their origin can be traced either to the spin-dependent scattering of electrons by randomly distributed impurities, referred to as extrinsic phenomena [31–35], or to the relativistic electronic structure of the material, where disorder plays a secondary role, referred to as intrinsic phenomena. For example, graphene exhibits an extrinsic SHE in the presence of local spin-orbit interaction via the skew scattering mechanism [36] and a quantized intrinsic spin Hall conductivity associated with the Z_2 topological invariant [37]. The same reasoning applies to the ISGE, which can be generated either by random sources of SOC via the anisotropic spin-precession mechanism [38], or by the uniform Rashba SOC [39].

The latter has served as a paradigmatic model system for studying the ISGE and has undergone extensive theoretical scrutiny, leading to significant developments over the years, although the ISGE itself has received less attention compared to the SHE. After the earliest results revealed the possibility of generating an in-plane spin polarization perpendicular to an applied static voltage in two-dimensional electron gases (2DEGs) [40–42], successively also observed in nonmagnetic interfaces [42], lanthanum aluminum oxide (LAO) and strontium titanium oxide (STO) systems [43], and topological insulators [44,45], a space-time dependent drift-diffusion theory has been formulated [46–48]. This framework was later extended to surface states of topological insulators [49], engineered graphene systems [50], and van der Waals heterostructures [51], the latter revealing the possibility of generating twist angle controlled spin polarization at an arbitrary angle with respect to the applied field.

Published by the American Physical Society under the terms of the Creative Commons Attribution 4.0 International license. Further distribution of this work must maintain attribution to the author(s) and the published article's title, journal citation, and DOI.

This paper focuses on a generalization of the conventional disordered Rashba model accounting for anisotropies in the effective mass and the linear Rashba parameter, as well as third-order warping terms, which are allowed in systems with C_{2v} and C_{3v} symmetry, respectively. The investigation of spintronic phenomena in such systems has recently attracted interest, as sizable anisotropies with linear Rashba SOC have been predicted in surface states of fcc crystals along the (1 1 0) direction [52], e.g., Au(1 1 0), and transition metal dichalcogenide (TMD) alloys of the form $MoS_{2(1-x)}Se_{2x}$ [53], as well as observed in tellurium–noble metal interfaces [54] and in (Tl, Au)/Si(1 0 0) compounds [55]. In addition, systems with third-order warping have been predicted in surface states of three-dimensional topological insulators (TIs) [56,57] and observed in Bi(1 1 1) [58]. Although we will not discuss in the present paper the microscopic details in real materials, it is worth mentioning that the description of spin splitting in surface states may be quite complex and may involve further effects besides the Rashba SOC [59,60].

The problem of an anisotropic Rashba SOC has been addressed only rarely and without comprehensive detail in the literature [61–64], mostly focusing on the dependence on the Fermi energy and being confined to the relaxation time approximation (RTA) [65], where transport lifetimes are replaced by mere constant values. In this regard, linear response theory is the main formalism adopted to investigate such transport phenomena. It is typically reduced to two main techniques: the Boltzmann equation (BE) [66], with its extensions [67–70], and the Kubo formula [71–74]. The former is strictly valid in the dilute limit, which provides the leading contribution to the system's response, while the latter provides a complete quantum-mechanical description of the system, incorporating geometrical Berry phase effects [75] and impurity-related quantum processes [76,77]. In the semiclassical limit, which is the regime considered in this work, there exists an exact correspondence between the two frameworks [78,79]: the self-consistent solution of the BE, which determines the transport lifetimes describing the out of equilibrium distortion of the distribution function, translates into the vertex renormalization in the Kubo formalism, together with the proper evaluation of the Green's function (GF) self-energy. Due to the challenging calculations required for a consistent treatment of disorder, the BE is often solved within the RTA. This corresponds to the constant broadening approximation (CBA) in the Kubo formalism [78,80,81], in which vertex corrections are totally ignored. However, this uncontrolled approximation is often seriously problematic. A well-known example is the SHE in 2DEGs: while neglecting the vertex corrections predicts a finite spin Hall conductivity, proper calculations reveal a vanishing response [82–85].

This paper represents another such case. We will show that the contribution of mass anisotropies to the ISGE cancels exactly once vertex corrections are taken into account, opposite to what is currently predicted by the literature [64]. In contrast, Rashba anisotropies make the ISGE itself anisotropic, influencing both its magnitude and orientation depending on the direction of the applied electric field. As a result, since the direction of the magnetization is generally no longer perpendicular to the electric current, we propose leveraging this deviation for direct experimental measurements of Rashba anisotropies. Our analysis employs both the Kubo formalism and the BE approach, with the former yielding analytical results and the latter numerical ones.

The remainder of this paper is organized as follows. In Sec. II we present the model Hamiltonian, briefly review the Kubo formalism used for the analytic calculations, and describe the numerical implementation of the BE. Moreover, here we clarify the connection between the RTA and the CBA. Section III is devoted to the calculation of the spin density–charge current response, hereafter referred to as spin-current response for brevity. We first reproduce the literature results for mass and Rashba anisotropies independently within the CBA. Then we extend the analysis by including the vertex corrections and the microscopic parameter-dependent self-energy in the Kubo formalism, coupled with the numerical solution of the BE beyond RTA. Finally, we investigate the effect of anisotropic warping in systems with C_{3v} symmetry. In Sec. IV we present our conclusions.

II. MODEL SYSTEM AND METHODOLOGY

The anisotropic Rashba model for 2DEG systems with C_{2v} symmetry can be described by the low-energy Hamiltonian [52]

$$H = \frac{p_x^2}{2m_x} + \frac{p_y^2}{2m_y} + \alpha_y p_y s_x - \alpha_x p_x s_y, \tag{1}$$

where $m_{x\,(y)}$ is the effective mass along the x (y) axis and s_i is a Pauli matrix i. Due to Rashba splitting, spin degeneracy is lifted, and the energy eigenvalues form two shifted parabolas, distorted by both mass and Rashba anisotropies:

$$\varepsilon_{\pm}(p_x, p_y) = \frac{p_x^2}{2m_x} + \frac{p_y^2}{2m_y} \pm \sqrt{(\alpha_y p_x)^2 + (\alpha_x p_y)^2}. \tag{2}$$

Analogously, we can define two distinct energy branches corresponding to an upper and lower band. The Fermi energy can then be positioned in such a way to intersect either a single branch (regime I) or both branches (regime II). In what follows, we will focus on the latter case, where the Fermi surface consists of two deformed disks with spin locked and perpendicular to the electron momentum. In this regime, the spin textures of the lower and upper bands wind in opposite directions, anticlockwise and clockwise, respectively (see Fig. 1).

Equation (1) is the starting point for our linear response calculations, whose technical details will be presented below. Assuming a slowly varying electric field $\mathbf{E}$ in both space and time, the spin density response takes the form

$$S_\alpha = K_{\alpha\beta} E_\beta, \tag{3}$$

where $K_{\alpha\beta}$ is the 3×2 spin-current linear response (LR) tensor, $\alpha = x, y, z$, $\beta = x, y$, and the Einstein summation rule is assumed. The impurity landscape enters the system Hamiltonian via an impurity potential of the form

$$V(\mathbf{x}) = \sum_i W(\mathbf{x} - \mathbf{x}_i), \tag{4}$$

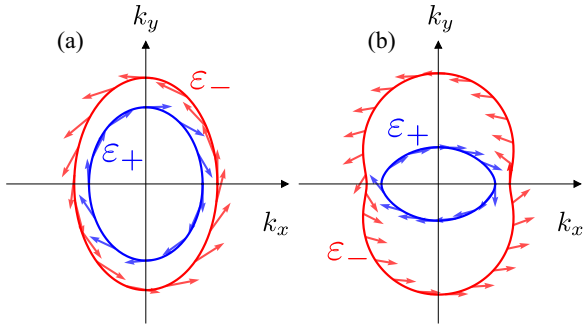


FIG. 1. Fermi surfaces obtained from Eq. (1) in regime II with anisotropic mass (a) and spin (b) terms. The lower and upper bands, corresponding to the outer (red) and inner (blue) curves, are labeled ε_- and ε_+, respectively. The direction of the arrows indicates the spin expectation values. Mass anisotropy is characterized by the ratio $m_y/m_x = 2$, while the Rashba coupling anisotropy is defined by $\alpha_y/\alpha_x = 5$. Parameters: $m = 0.27\, m_e$, with m_e being the electron mass, $\alpha = 0.66\,\text{eV Å}$, and Fermi energy $\varepsilon_f = 0.475\,\text{eV}$. The Rashba splitting is $\sim$0.12 eV.With these numerical parameters, the maximum value of the Fermi momentum obtained across both plots is 0.3 Å^{-1}, while the minimum is 0.1 Å^{-1}.

where $W(\mathbf{x}-\mathbf{x}_i) = u_0 \sum_i R^2 \delta(\mathbf{x}-\mathbf{x}_i)$ is the potential of a single short-range nonmagnetic impurity located at position $\mathbf{x}_i$, u_0 is the strength of a single impurity potential, and R is the characteristic length scale of the impurity potential's range [30]. For simplicity, we set $R = 1$ for analytic expressions hereafter.

The Kubo formula and diagrammatic theory. Within the Kubo formalism, the disorder-averaged spin-current response can be separated into two components, a Fermi sea and a Fermi surface [86]. Restricting our analysis to the dilute limit, wherein the impurity concentration $n_i \ll 1$, we can extract the leading contribution to the spin-current response $\sim 1/n_i$ by safely neglecting the Fermi sea term and products of the GF belonging to the same sector, i.e., retarded or advanced, [36], finally obtaining the Kubo-Streda formula [87,88],

$$K_{\alpha\beta} = \frac{1}{2\pi}\int \frac{d\mathbf{p}}{(2\pi)^2}\,\mathrm{tr}\left\langle\left[\frac{s_\alpha}{2} G^R_{\mathbf{p}} j_\beta G^A_{\mathbf{p}}\right]\right\rangle_{\text{dis}}, \tag{5}$$

where the trace is over the internal matrix indices; $j_\beta = \partial H/\partial p_\beta$ is the electric current operator, i.e., here defined without the electric charge $-e$; $G^{R(A)}_{\mathbf{p}} = 1/(\varepsilon - H \pm i0^+)$ is the clean retarded (advanced) GF; and we made use of natural units $\hbar \equiv 1 \equiv e$.

Disorder averaging, here assumed to be within the first Born approximation (FBA) [78], is denoted by $\langle\ldots\rangle_{\text{dis}}$. Using the standard rules of diagrammatics [89] (or functional approaches to nonequilibrium field-theory methods [90]), Eq. (5) becomes

$$K_{\alpha\beta} = \frac{1}{2\pi}\int \frac{d\mathbf{p}}{(2\pi)^2}\,\mathrm{tr}\left[\frac{s_\alpha}{2}\mathcal{G}^R_{\mathbf{p}}\tilde{J}_\beta\mathcal{G}^A_{\mathbf{p}}\right], \tag{6}$$

depicted in Fig. 2(a) as a dressed bubble, where $\tilde{J}_\beta$ is the renormalized current vertex and

$$\mathcal{G}^{R(A)}_{\mathbf{p}} = \frac{1}{\varepsilon - H - \Sigma^{R(A)}} \tag{7}$$

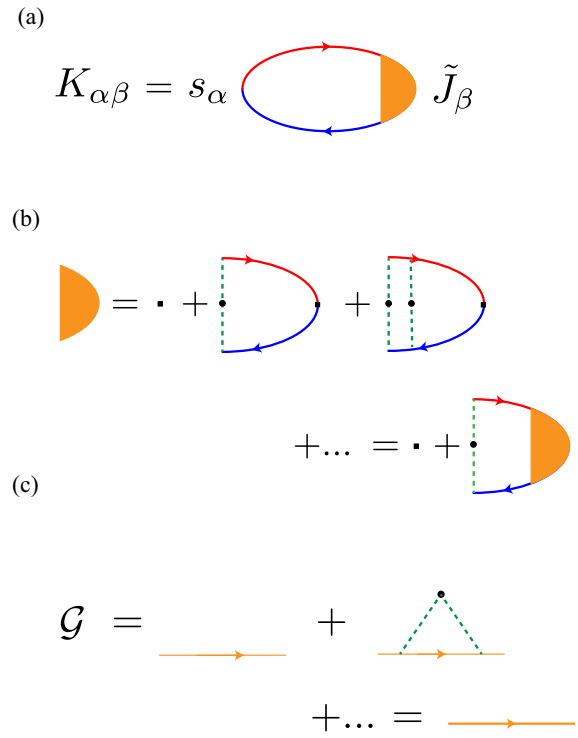


FIG. 2. Diagrammatic representation of the spin-current response function. The impurity-averaged bubble in (a) depicts the Kubo formula, where blue and red solid lines with arrows represent the advanced and retarded GF sectors, respectively. The dressed vertex is indicated by orange shading. Its skeleton expansion is shown in (b), where the dashed green lines denote the averaged interaction with a single impurity, represented by a black dot. The bare current vertex is identified by a black square. (c) Expansion of the GF within the FBA, where thin lines denote bare GFs and thick lines denote dressed GFs.

is the disorder-averaged retarded (advanced) GF. Under the FBA, the leading contribution to the self-energy in impurity concentration is given by

$$\Sigma^{R(A)} = n_i u_0^2 g_0^{R(A)}, \tag{8}$$

with $g_0^{R(A)}$ being the momentum-integrated clean GF; see Fig. 2(c). Consistently, the renormalized vertex is given by the Bethe-Salpeter integral equation [82,91–93],

$$\tilde{J}_\beta = j_\beta + n_i u_0^2 \int \frac{d\mathbf{p}}{(2\pi)^2}\mathcal{G}^R_{\mathbf{p}}\tilde{J}_\beta\mathcal{G}^A_{\mathbf{p}}, \tag{9}$$

corresponding to the noncrossing ladder series of impurity scattering, illustrated in Fig. 2(b). A convenient way to solve Eq. (9) is to separate the renormalized vertex into the bare, momentum-*dependent* term j_β and the momentum-*independent* correction δJ_β, such that $\tilde{J}_\beta = j_\beta + \delta J_\beta$ [30]. The result is a Bethe-Salpeter equation for δJ_β,

$$\delta J_\beta = \delta\bar{J}_\beta + n_i u_0^2 \int \frac{d\mathbf{p}}{(2\pi)^2}\mathcal{G}^R_{\mathbf{p}}\delta J_\beta\mathcal{G}^A_{\mathbf{p}}, \tag{10}$$

where $\delta\bar{J}_\beta = n_i u_0^2 \sum_{\mathbf{p}} \mathcal{G}^R_{\mathbf{p}} j_\beta \mathcal{G}^A_{\mathbf{p}}$ is the first-order correction to the current operator. Since the displacement of the current operator in Eq. (10) is momentum independent, it can be factored out, allowing the equation to be solved explicitly,

although this is generally a difficult task [93]. The dressed vertex is obtained as

$$\delta J_\beta = \mathcal{D}_{\beta\nu}\delta\bar{J}_\nu, \tag{11}$$

where

$$\mathcal{D}^{-1}_{\mu\nu} = \delta_{\mu\nu} - \frac{n_i u_0^2}{2}\mathcal{N}_{\mu\nu} \tag{12}$$

is called *diffuson* and $\mathcal{N}_{\mu\nu} = \int \frac{d\mathbf{p}}{(2\pi)^2}\mathrm{tr}[s_\mu \mathcal{G}^R_{\mathbf{p}} s_\nu \mathcal{G}^A_{\mathbf{p}}]$. Once Eq. (12) is evaluated, the dressed current vertex is fully determined, and the Kubo formula is thereby completely specified. This approach conveniently eliminates the need for any ansatz for $\tilde{J}_\beta$, making the method a transparent and general algorithm for obtaining analytical solutions to transport problems. However, implementing it is far from being easy, especially in the presence of band anisotropies, which make momentum integrations nontrivial.

Quantum kinetic theory (QKT). A recently developed QKT approach [79,94], based on the Keldysh-Larkin-Ovchinnikov technique [95,96], enables a rigorous, systematic inclusion of impurity-induced semiclassical mechanisms, quantum corrections, and topological effects within the linear response theory, with no need for explicit diagrammatic expansions, but solely relying on the self-energy expression [79]. This method has the advantage of providing a clearer physical understanding of the problem under investigation, enabling more streamlined practical calculations, establishing a formal connection with the Kubo formalism, and incorporating macroscopic finite size effects [97].

In the present case, restricting our interest to the system semiclassical steady-state response, the method translates into a set of N_b linear Boltzmann equations (BEs),

$$\mathbf{E}\cdot\partial_{\mathbf{p}}\varepsilon_{\mathbf{p},n}\,\partial_\varepsilon f^{(\mathrm{eq})}_{\mathbf{p},n} = I_n, \tag{13}$$

where N_b is the number of bands in the system, n and m are band indices, $\varepsilon_{\mathbf{p},n}$ denotes the eigenvalue in momentum space of the nth band, and $f^{(\mathrm{eq})}_{\mathbf{p},n}$ is the equilibrium Fermi-Dirac distribution. The collisional integral I_n, which arises from the disorder-induced self-energy for the Keldysh Green function, takes the form

$$I_n = \sum_m \int \frac{d\mathbf{p}'}{(2\pi)^2}\delta(\varepsilon_{\mathbf{p}',m} - \varepsilon_{\mathbf{p},n})(\delta f_{\mathbf{p}',m} - \delta f_{\mathbf{p},n})W_{nm} \tag{14}$$

with

$$W_{nm} = 2\pi n_i u_0^2 \mathrm{tr}[\hat{P}_{\mathbf{p},n}\hat{P}_{\mathbf{p}',m}] \tag{15}$$

being the scattering kernel, $\hat{P}_{\mathbf{p},n}$ the projector into the eigenspace identified by $\varepsilon_{\mathbf{p},n}$, and $\delta f_{\mathbf{p},n}$ the linear displacement of the occupation function of the nth band, i.e., $f_{\mathbf{p},n} = f^{(\mathrm{eq})}_{\mathbf{p},n} + \delta f_{\mathbf{p},n}$. Once Eq. (13) is solved, the observable of interest, which, in our case, corresponds to the spin density, is calculated, at leading order $\sim 1/n_i$, as

$$S_\alpha = \sum_n \int \frac{d\mathbf{p}}{(2\pi)^2}\mathrm{tr}\Big[(f_{\mathbf{p},n}\hat{P}_{\mathbf{p},n})\frac{s_\alpha}{2}\Big], \tag{16}$$

which takes the form of Eq. (3). As shown in Ref. [79] subleading corrections $\sim(n_i)^0$ can also be obtained by evaluating the off-diagonal, in the energy basis, matrix elements of the density matrix. However, there is no need to consider them for the evaluation of the spin response.

In concrete analytic calculations, the system of BEs can be solved in two ways: (i) by making an ansatz for the out of equilibrium distribution function, or (ii) by solving the equations iteratively in a Bethe-Salpeter fashion. Often, the first-order correction suggests the suitable ansatz. The former method ideally closes the system of equations, making them solvable [36], while the latter is traditionally approached using the RTA. This commonly adopted procedure solves Eq. (13) at first order—thus neglecting the contribution $\sim\delta f_{\mathbf{p}',m}$ in Eq. (14), often referred to as a *scatter-in* term [65]—and replaces the resulting integral with a constant transport time $1/\tau$, i.e., $I_n \to -\delta f_{\mathbf{p},n}/\tau$. The combination of these crude assumptions can be problematic, as they lose details of the scattering mechanisms in play, which depend on both the bare system Hamiltonian and the impurity structure. The early success of the RTA is a result of its application to specific, paradigmatic systems, e.g., single-band Hamiltonians with scalar electrostatic impurities. In such cases, the linear displacement of the occupation function is proportional to the scalar product between the group velocity, $\partial_{\mathbf{p}}\varepsilon_{\mathbf{p},n} = \mathbf{v}_n$, and the electric field, i.e., $\sim\cos\theta$, while the scattering kernel is momentum independent. Consequently, the momentum integration defining scatter-in term in Eq. (14) vanishes, thereby validating the RTA. However, its validity is compromised in multiband systems, such as in the present case, where the influence of SOC during scattering events renders the scattering kernel momentum dependent and the scatter-in term nonvanishing.

Our QKT environment allows us to frame both approximations within the Kubo formalism. According to Ref. [79], the out of equilibrium occupation function at the leading order in the impurity concentration takes the form

$$f_{\mathbf{p},n} = -\partial_\varepsilon f^{(\mathrm{eq})}_{\mathbf{p},n}\tau_n \sum_i \mathbf{E}\cdot\tilde{\mathbf{J}}_n, \tag{17}$$

where $\mathrm{i}/2\tau_n = \mathrm{Im}\Sigma^A_n$, with Σ^A_n and $\tilde{\mathbf{J}}_n$ being, respectively, the advanced GF self-energy and the renormalized vertex shown in Eqs. (7) and (9), projected on the nth band. This expression can be directly compared with the RTA solution of the BE:

$$f^{\mathrm{RTA}}_{\mathbf{p},n} = -\partial_\varepsilon f^{(\mathrm{eq})}_{\mathbf{p},n}\tau \sum_i \mathbf{E}\cdot\mathbf{j}_n, \tag{18}$$

clarifying the meaning of the RTA within the diagrammatic language: it corresponds to neglecting vertex renormalization in the Bethe-Salpeter equation and replacing the self-energy with a constant independent of the Hamiltonian and impurity structure. The former approximation, as extensively discussed in the literature, has proved inadequate for Hamiltonians with nontrivial structures in spin space [82], while the latter effectively neglects the shape of the density of states (DOS), which is particularly questionable here, since the DOS encodes information on the anisotropy.

The need of surpassing the RTA motivated us to develop a numerical algorithm for the exact solution of Eq. (13). In contrast to the Kubo-Streda formula, where the GFs introduce discontinuities in momentum space, which are tricky to handle, this approach is particularly suitable for numerical

integrations, thanks to the Fermi surfaces' sole contribution to the linear response within the BEs. In particular, the occupation number takes the form

$$\delta f_{\mathbf{p},n} = -\delta(\varepsilon_{\mathbf{p},n} - \varepsilon_{\mathrm{F}}) g_{\mathbf{p},n}, \tag{19}$$

with ε_F being the Fermi energy. While analytical approaches typically need an ansatz for the angular dependence of the distribution function [36,38,98], Eq. (19) shows the most general structure for the occupation number, as the coefficients $g_{\mathbf{p},n}$ retain full information of both the absolute value of the momentum and its direction. Inserting our ansatz in Eq. (14), the BE for band n takes the form

$$\mathbf{E}\cdot\mathbf{v}_n(\phi) = \sum_m \int \frac{d\phi'\,\mathrm{k}_m}{(2\pi)^2}\left(\frac{g_m}{\mathrm{v}_m}(\phi') - \frac{g_n}{\mathrm{v}_n}(\phi)\right) W_{nm}(\phi,\phi'), \tag{20}$$

where all quantities are evaluated at Fermi energy; e.g., k_m and v_n are, respectively, the absolute value of the Fermi momentum in band m and the group velocity for band n at the Fermi level. We now discretize the Fermi surfaces in N_θ angular steps and, accordingly, all the elements in Eq. (20), with the aim of rewriting the right-hand side of the BE as a Riemann sum. In matrix form, Eq. (20) can finally be written as [99]

$$\mathbf{E}\cdot\bar{\mathbf{v}} = \hat{\mathrm{S}}\,\bar{g}, \tag{21}$$

where $\bar{g}$ and each component of $\bar{\mathbf{v}}$ are column vectors of dimension $N = N_b \times N_\theta$, and $\hat{\mathrm{S}}$ is the collisional integral expressed as an $N \times N$ matrix. The occupation number is then obtained as

$$\bar{g} = \hat{\mathrm{S}}^{+}\mathbf{E}\cdot\bar{\mathbf{v}}_n, \tag{22}$$

with $\hat{\mathrm{S}}^{+}$ denoting the *pseudoinverse* of $\hat{\mathrm{S}}$. A standard inversion is infeasible, since LR theory imposes the condition

$$\sum_n \int \frac{d\mathbf{p}}{(2\pi)^2}\delta f_{\mathbf{p},n} = 0. \tag{23}$$

This reflects the fact that summing the distribution function over all degrees of freedom yields the number of particles, a condition already satisfied by $f^{(\mathrm{eq})}_{\mathbf{p}}$. Ultimately, this renders the system of BEs overdetermined.

III. RESULTS AND DISCUSSION

In this section, we evaluate the spin-current response of two classes of materials belonging to the C_{3v} and C_{2v} point groups. Both classes lack inversion symmetry along the $\hat{z}$ axis, and allowing the Rashba SOC, are invariant across the vertical mirror plane, and are invariant under threefold and twofold rotations about the $\hat{z}$ axis, respectively [13]. Concerning C_{2v} materials, to make the problem more analytically tractable and, at the same time, to better understand the roles of mass and Rashba anisotropies, we analyze these two cases separately: $m_x \neq m_y$ with $\alpha_x = \alpha_y = \alpha$, and $m_x = m_y = m$ with $\alpha_x \neq \alpha_y$. Each analytical result obtained via the Kubo formalism, Eq. (6), is validated through a numerical check implemented with the BE, Eqs. (16) and (21). We consider this dual evaluation essential, as anisotropic Fermi surfaces lead to nontrivial momentum integrations, often requiring systematic Taylor expansions in the anisotropy parameters within the Kubo formalism which grow the algebraic complexity.

A. Review of the CBA

In what follows, we estimate the spin-current response within the CBA. The GFs self-energy, previously defined in Eq. (8), is replaced by a constant independent of anisotropy, $\Sigma^{R(A)} \to -\mathrm{i}/2\tilde{\tau}$, with the momentum relaxation time $\tilde{\tau}$ having the units of time and being inversely proportional to the impurity-related factor $n_i u_0^2$. In addition the vertex corrections are ruled out, requiring that $\tilde{J}_\beta \to j_\beta$ in Eq. (6). Considering, for simplicity, an electric field applied along the x axis, the current operator is

$$j_x = \frac{p_x}{m_x} - \alpha s_y \tag{24}$$

in case (i), and

$$j_x = \frac{p_x}{m} - \alpha_x s_y \tag{25}$$

in case (ii).

For computational purposes, it is convenient to decompose the GFs into their spin components, $\mathcal{G}_i^{R(A)} = (1/2)\mathrm{tr}[\mathcal{G}^{R(A)}s_i]$, with $i = 0, x, y$, where each element is directly related to the projected GFs (PGFs), $\mathcal{G}_\pm^{R(A)}$, on the two bands ε_+ and ε_-. To show this, we express the Hamiltonian in the compact form

$$H = h_0 s_0 + \mathbf{h}\cdot\mathbf{s}, \tag{26}$$

where h_0 is the kinetic term, $\mathbf{s}$ is the vector of Pauli matrices, and $\mathbf{h} = (\alpha_y p_y, -\alpha_x p_x, 0)$ is the effective magnetic field induced by the Rashba SOC. The two projectors associated to the helicity bands are $P_\pm = (s_0 \pm \hat{\mathbf{h}}\cdot\mathbf{s})/2$, allowing us to rewrite the GFs as

$$\mathcal{G}^{R(A)} = (\mathcal{G}_+^{R(A)} + \mathcal{G}_-^{R(A)})\frac{s_0}{2} + (\mathcal{G}_+^{R(A)} - \mathcal{G}_-^{R(A)})\frac{\hat{\mathrm{h}}\cdot\mathbf{s}}{2}, \tag{27}$$

where $\hat{\mathbf{h}} = \mathbf{h}/|\mathbf{h}|$ and

$$|\mathbf{h}| = \sqrt{(\alpha_x p_x)^2 + (\alpha_y p_y)^2} \tag{28}$$

are the direction and module of the effective magnetic field, respecively. The Kubo-Streda formula can then be expressed in terms of the products of PGFs, $\sim \sum_{i,j\in\{-,+\}} \mathcal{G}_i^R \mathcal{G}_j^A$, where only the *intraband* terms, $\sim \mathcal{G}_\pm^R \mathcal{G}_\pm^A$, are retained. *Interband* elements, which describe transitions between different bands at the same momentum and thus account for effects outside the Fermi surface, contribute to the response function only beyond leading order [100]. This can be understood by considering that, in the weak disorder limit, $\tilde{\tau} \to \infty$, and the retarded and advanced PGFs have poles with real parts differing by the interband energy difference, which is larger than disorder broadening at the same momentum. As a consequence interband integrals are generically smaller than intraband ones by a factor of $\sim\hbar/(\Delta E\tilde{\tau})$, ΔE being an interband energy difference. What remains exists only within the Fermi surface, valid in the semiclassical regime, in accordance with Eq. (20). To see this explicitly, we can express products between PGFs to the leading order in the impurity concentration as

$$\mathcal{G}_\pm^R \mathcal{G}_\pm^A = \mathrm{i}\tilde{\tau}(\mathcal{G}_\pm^R - \mathcal{G}_\pm^A) = -2\pi\,\tilde{\tau}\,\delta(\varepsilon_{\mathrm{F}} - \varepsilon_{\mathbf{p},n}), \tag{29}$$

essentially playing the role of Eq. (18) for the BE. The calculation of the Kubo-Streda formula is now greatly simplified,

as the delta function in Eq. (29) constrains the momentum integration within the Fermi surfaces. The remaining angular integration is readily performed through standard techniques, such as as the application of the residue theorem after mapping the angle to a complex variable [64], finally giving the result

$$K_{yx}^{(\mathrm{i})} = \frac{m_y \alpha \tilde{\tau}}{2\pi\left(1+\sqrt{\frac{m_y}{m_x}}\right)}, \tag{30}$$

in case (i), and

$$K_{yx}^{(\mathrm{ii})} = \frac{\alpha_y m \tilde{\tau}}{2\pi\left(1+\frac{\alpha_y}{\alpha_x}\right)}, \tag{31}$$

in case (ii) in accordance with the literature [64].

Equations (30) and (31) clearly show a dependency of the transverse spin response on the anisotropy parameters, controlled by the ratio between the masses and the Rashba couplings along the perpendicular axis. Apparently, tuning this ratio provides additional control over the response intensity compared to the isotropic case. However, the constant relaxation time $\tilde{\tau}$ is suspiciously independent of anisotropy, although, being proportional to the DOS, it should reflect such dependency. Should this be the case, the responses' behavior in Eqs. (30) and (31) could be radically different. In the following sections, we will compute the spin-current response following the prescriptions in Sec. II and compare the outcomes with the results found in this section.

B. Full inclusion of the vertex corrections beyond the CBA: Mass anisotropy

Focusing on mass anisotropy and resuming our last comment, we need to clarify the dependence of the self-energy on anisotropy. This is a relatively easy task, the result being

$$\Sigma^{\mathrm{R(A)}} = \mp\frac{\mathrm{i}}{2} n_i u_0^2 \sqrt{m_x m_y}\, s_0, \tag{32}$$

where only the anti-Hermitian part of the self-energy has been retained. As expected intuitively, the relaxation time depends simultaneously on m_x and m_y, as does the DOS, thereby invalidating the naive application of the CBA with a constant factor $\tilde{\tau}$. Our following goal is to evaluate the Kubo-Streda formula with the renormalized current vertex.

Courtesy of the simple Hamiltonian structure, this task is feasible analytically with the help of a straightforward rearrangement of Eq. (9),

$$\tilde{J}_x = \frac{p_x}{m_x} + \Gamma_x, \tag{33}$$

where

$$\begin{aligned}\Gamma_x = & -\alpha s_y + n_i u_0^2 \int \frac{d\mathbf{p}}{(2\pi)^2} \mathcal{G}_{\mathbf{p}}^{\mathrm{R}} \frac{p_x}{m_x} \mathcal{G}_{\mathbf{p}}^{\mathrm{A}} \\ & + n_i u_0^2 \int \frac{d\mathbf{p}}{(2\pi)^2} \mathcal{G}_{\mathbf{p}}^{\mathrm{R}} \Gamma_x \mathcal{G}_{\mathbf{p}}^{\mathrm{A}}\end{aligned} \tag{34}$$

is the momentum-independent part of the renormalized vertex entering the Bethe-Salpeter equation. Following the same decomposition scheme employed in Sec. III A, we find that the second term on the right-hand side of Eq. (34), being equal to αs_y to the lowest order in the impurity concentration, exactly cancels the first term. Remarkably, this is allowed by a nontrivial compensation between the anisotropy carried by the self-energy and that contained in the DOS; this information is completely lost in the RTA. A detailed evaluation of the above second term is carried out in the Appendix. As a result, the Bethe-Salpeter equation (34) has the trivial solution $\Gamma_x = 0$, and the renormalized vertex reduces to

$$\tilde{J}_x = \frac{p_x}{m_x}, \tag{35}$$

which is the bare vertex in the absence of Rashba coupling. This is a striking but well-known result, already established in the literature [82], displaying an additional deviation from the RTA. The physical origin of the vertex corrections stems from the eigenstate texture (spin eigenstate in the present case) in momentum space: the *s*-wave isotropic disorder potential becomes dependent on momentum transfer upon its transformation in the basis of the Hamiltonian eigenstates [92]. In the present case, the vertex correction in the second term in the right-hand side of Eq. (34) may be interpreted as the averaged momentum in the displaced Rashba energy bands. More in general, conservation laws and Ward identities may be shown to constrain vertex functions and self-energies [101]. Combining these results, the spin-current response becomes

$$K_{yx} = \frac{\alpha}{2\pi n_i u_0^2}, \tag{36}$$

which coincides with the traditional ISGE [35]. In other words, mass anisotropy leaves the spin-current response unaffected at the semiclassical level, in contrast with current knowledge. The numerical approach based on QKT confirms this outcome, in agreement with our analytic analysis. On physical grounds, in retrospect, the above result is not surprising, given the fact the ISGE can be seen as the spin-current response to the internal Rashba magnetic field induced by the distortion of the Fermi surface in the presence of an applied electric field. This also provides another example, beyond the SHE in 2DEGs [82], where vertex correction does not merely refine transport times but fundamentally changes the transport *phenomenology* of the studied system.

C. Full inclusion of the vertex corrections beyond the CBA: Rashba anisotropy

The considerations presented in the previous section can be reproduced here in full, especially the expression for the renormalized current vertex given in Eq. (34), with $\alpha \to \alpha_x$ and $m_x \to m$. In fact, once again we find that the second term on the right-hand side, which equals $\alpha_x s_y$, exactly cancels the first. As a result, the renormalized current reduces to the bare vertex in the absence of Rashba SOC, Eq. (35). This may seem surprising, because the GFs self-energy loses its anisotropic character, simply becoming $\sim \mathrm{i} n_i u_0^2 m$, and therefore no longer compensates the anisotropy of the DOS. However, its role is taken over by the magnitude of the effective magnetic field $|\mathbf{h}|$, Eq. (28), explicitly appearing in the off-diagonal part of the GFs and to which the DOS is proportional. Using these results in the Kubo formula, we finally find

$$\mathbf{S} = \frac{\hat{\alpha}\,\mathbf{E}}{2\pi n_i u_0^2}, \tag{37}$$

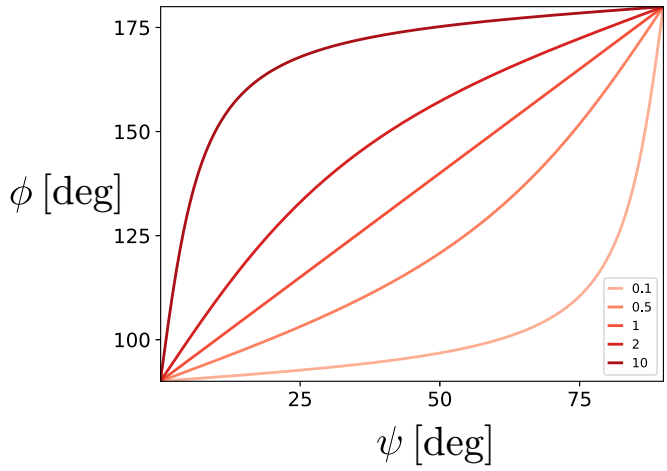


FIG. 3. Inclination of the spin density as a function of the applied electric field angle ψ and the ratio $\alpha_r = \alpha_y/\alpha_x$. Each curve corresponds to a different value of α_r, as indicated in the legend. The plots are computed numerically and are in perfect agreement with the analytical result given in Eq. (39).

where

$$\hat{\alpha} = \begin{pmatrix} 0 & -\alpha_y \\ \alpha_x & 0 \end{pmatrix}. \tag{38}$$

The functional dependence of **S** from the physical parameters in play is the same as the conventional ISGE, $\mathbf{S}^{\text{iso}}$, which is explicitly recovered either when the electric field is applied along a principal axis or when Rashba isotropy is restored. The distinction between the contribution of the different Rashba constants now becomes apparent, whereas it remained unseen in the isotropic case, with important consequences for the transport properties of the system. First, the magnitude of the spin density depends on the ratio between α_x and α_y. For example, assuming $\alpha_x \neq 0$ and an electric field applied at an angle of $\pi/4$, we obtain $\mathrm{S} = \frac{\alpha_x E}{\sqrt{2}}\sqrt{1 + (\alpha_y/\alpha_x)}$, which exceeds S^{iso} if $\alpha_y > \alpha_x$ or remains lower otherwise. Second, the direction of the spin density is no longer, in general, perpendicular to the electric field, but follows the law

$$\phi = \arctan\left(-\frac{\alpha_x}{\alpha_y}\cot\psi\right) + \pi, \tag{39}$$

where $\phi = \arctan(\frac{S_y}{S_x})$ and $\psi = \arctan(\frac{E_y}{E_x})$. Clearly, if $\alpha_x = \alpha_y$, then $\phi = \psi + \pi/2$, that is the conventional ISGE, where the spin density is perpendicular to the applied electric field. The direction of the induced spin polarization and its dependence on the direction of the applied electric field can be measured as it has been done for InGaAS epilayers [102].

The validity of Eq. (39) is tested numerically with the Boltzmann formalism, and is depicted in Fig. 3, wherein we find a *perfect match* with the analytical result. The plots in Fig. 3 indicate that for small values of α_y/α_x and ψ, the spin density is mainly transverse to the applied field, but as the ratio increases, it progressively aligns with the electric field. Conversely, for $\psi \to \pi/2$, the behavior is reversed. Beyond the fascinating deviation of this phenomenon from the conventional ISGE, the precise relation between the direction of the spin density and the ratio between the Rashba couplings can be exploited experimentally: a purely electrical excitation of the material indicates the degree of anisotropy of the Rashba coupling.

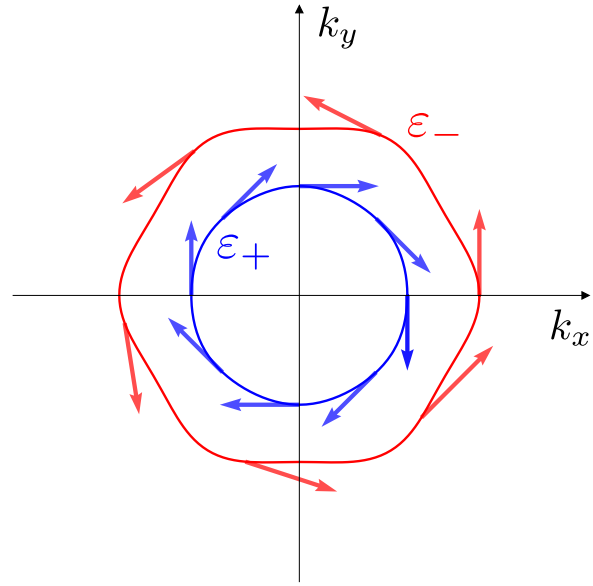


FIG. 4. Fermi surfaces of a 2DEG with C_{3v} symmetry in the presence of a warping term, Eq. (40). The figure is representative of Bi/Cu(1 1 1) systems [57], with $m = -0.29\,m_e$, $\alpha = 0.85\,\text{eV Å}$, $\lambda = 12\,\text{eV Å}^3$, and $\varepsilon_f = -0.215\,\text{eV}$. The Rashba splitting is $\sim 0.1\,\text{eV}$.

D. Warping term

As promised in the Introduction, we extend our analysis to include an additional source of anisotropy in the low-energy effective Hamiltonian considered in this paper, Eq. (1), which applies to a broad family of realistic materials of C_{3v} symmetry [57], ranging from 2DEGs to surface states of three-dimensional TIs. Such symmetry rules out the anisotropies considered in the former sections of this work, imposing that $m = m_x = m_y$, $\alpha = \alpha_x = \alpha_y$. In this scenario, the SOC gives rise to the warping term [56],

$$H_w = \frac{\lambda}{2}(p_+^3 + p_-^3)s_z, \tag{40}$$

where $p_\pm = p_x \pm i p_y$ and λ is the warping coupling strength, whose effect on the Fermi surfaces is illustrated in Fig. 4. The eigenvalues read

$$\varepsilon_\pm(p_x, p_y) = \frac{p^2}{2m} \pm \sqrt{\alpha^2 p^2 + \lambda^2 p^6 \cos^2(3\theta)} \tag{41}$$

with $\theta = \arctan(p_y/p_x)$ and, in contrast to systems with purely Rashba SOC (both isotropic and anisotropic), the eigenvectors in the presence of a warping term (40) acquire an out of plane spin component.

An analytic solution to the transport problem is intractable in this system, and therefore a fully numerical approach is needed. In particular, we adopted the numerical algorithm based on the QKT approach described in Sec. II. The result is shown in Fig. 5, which plots the predicted trend of the spin-current response as a function of the Rashba coupling

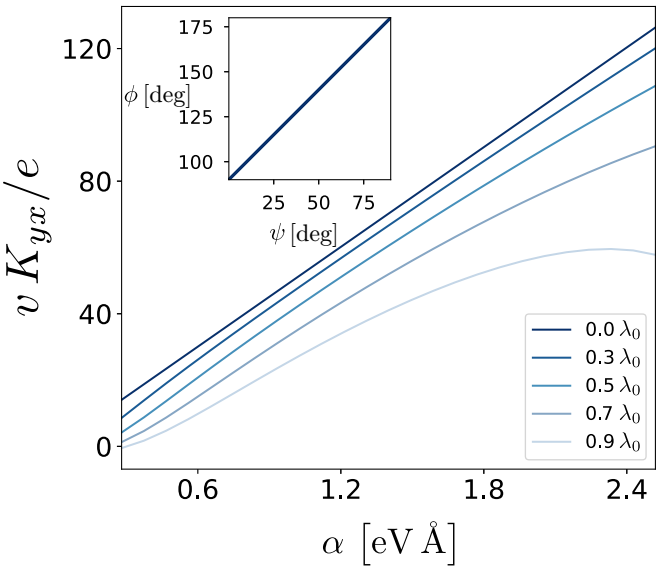


FIG. 5. Rashba coupling dependence of the current-induced spin-current response for different values of the warping constant λ, listed in the legend, with $\lambda_0 = 26.28\,\text{eV Å}^3$. The inset illustrates the spin density inclination against the applied electric field angle, revealing perfect perpendicularity for any value of λ, as in the case of the ISGE. The prototypical studied system is again Bi/Cu(1 1 1), introduced in Fig. 4, where $v = 5 \times 10^5\,\text{m/s}$ is the Fermi velocity. The other parameters are $n_i = 10^{16}\,\text{m}^{-2}$ and $u_0 = 0.1\,\text{eV nm}^2$.

strength and for different values of λ. In contrast to the Rashba anisotropy case, see Fig. 3, the inclusion of a warping term in the Hamiltonian preserves the direction of the spin density perpendicular to the applied electric field, as illustrated in the inset. For this reason, and without loss of generality, the main plot shows the spin response component along the y axis for an electric field applied along the x axis. One effect of the warping anisotropy is the systematic decrease of the spin-current response as the warping strength increases, which becomes more pronounced for large values of the Rashba constant. This is largely attributed to the out of plane rotation of the electrons' spin momentum at the Fermi surfaces and their departure from the ideal circular path, as pointed out in the literature [61]. A second effect we report is a progressive deviation from the linear dependence of the spin-current response on α, characteristic of the ISGE in 2DEGs, which further contributes to the decrease of the spin response.

IV. CONCLUSIONS

In this paper we had a fresh look at the influence of the lowering of the full rotational symmetry to the C_{2v} and C_{3v} symmetry groups on the inverse spin galvanic effect (ISGE) in the presence of Rashba SOC. At variance with previous investigations in the literature, we have established that vertex corrections are crucial and their subtle effect is not captured by constant broadening approximation. For instance, in the case of mass anisotropy, in contrast with previous reported results, we find that the ISGE remains unaffected. More, importantly, in the case of Rashba SOC anisotropy, the C_{2v} reduced symmetry manifests in a different strength for the ISGE along the two axes of the two-dimensional electron gas. In particular, in general for arbitrary direction of the electric field, the induced spin polarization is no longer simply perpendicular to the electric field but makes an angle larger or smaller than $\pi/2$ depending on the anisotropy ratio of the Rashba couplings. In the case of C_{3v} symmetry, the theoretical analysis has been a full numerical implementation of the general scheme provided by the QKT approach previously developed by two of the authors. In this respect our paper also shows, in a relatively simple Hamiltonian case, the feasibility of a general method to treat disorder effects beyond the often used constant broadening approximation.

ACKNOWLEDGMENTS

T.V. and R.R. thank Mairbek Chshiev, Jing Li, and Libor Vojáček for fruitful discussions. One of the authors (T.V.) acknowledges support by the EIC Pathfinder OPEN Grant No. 101129641 "OBELIX" and a France 2030 government grant managed by the French National Research Agency PEPR SPIN, Grant No. ANR-22-EXSP0009 (SPINTHEORY).

DATA AVAILABILITY

The data that support the findings of this article are not publicly available. The data are available from the authors upon reasonable request.

APPENDIX: EVALUATION OF AN INTEGRAL

In this Appendix we evaluate the integral appearing in the first line in the right-hand side of Eq. (34), which we report here for the sake of clarity:

$$n_i u_0^2 \int \frac{d\mathbf{p}}{(2\pi)^2} \mathcal{G}^R_{\mathbf{p}} \frac{p_x}{m_x} \mathcal{G}^A_{\mathbf{p}}. \tag{A1}$$

We evaluate the above integral by considering both mass and Rashba SOC anisotropy. To this end, it is convenient to define the following angle-dependent quantities:

$$m(\theta) = \frac{m_x m_y}{m_y \cos^2\theta + m_x \sin^2\theta}$$

and

$$\alpha(\theta) = \sqrt{(\alpha_x \cos\theta)^2 + (\alpha_y \sin\theta)^2}.$$

To evaluate the integral, we first observe that the factor p_x is odd upon momentum inversion and hence we only need to consider combinations of the components of the Green functions which are also odd. By considering the decomposition of each Green function as given by Eq. (27), the matrix structure of the integral reduces to only the matrix s_y with a numerical coefficient given by

$$\frac{n_i u_0^2}{\Sigma^R - \Sigma^A} \int \frac{d\mathbf{p}}{(2\pi)^2} \frac{p_x \hat{h}_y}{2m_x} (\mathcal{G}^R_+ - \mathcal{G}^A_+ - \mathcal{G}^R_- + \mathcal{G}^A_-).$$

By recalling that the self-energy scales as $n_i u_0^2$ [cf. Eq. (32)], one immediately recognizes that the integral, in the weak disorder limit, is independent of the disorder. To perform the momentum integration, we use polar coordinates

and make a change of variable from the absolute value of momentum to an energy variable,

$$\varepsilon_\pm = \frac{p^2}{2m(\theta)} \pm \alpha(\theta)p,$$

where the the $\pm$ sign is used in the integral involving the $\mathcal{G}_+^{R,A}$ and $\mathcal{G}_-^{R,A}$, respectively. At given $\varepsilon_\pm$, the absolute value of momentum reads

$$p_\pm = \mp m(\theta)\alpha(\theta) + \sqrt{[m(\theta)\alpha(\theta)]^2 + 2m(\theta)\varepsilon}$$

and the integral over $\varepsilon_\pm$ can be readily performed by the residues method. One then is left with the following angle integral,

$$\frac{n_i u_0^2}{\Sigma^R - \Sigma^A} \int_0^{2\pi} \frac{d\theta}{2\pi} \frac{\alpha_x \cos^2(\theta)}{m_x \alpha(\theta)} (-\mathrm{i}\, m^2(\theta)\alpha(\theta)),$$

where the term in parentheses in the integrand originates from the residue integration. Notice how the factors $\alpha(\theta)$ with the unpleasant square root of trigonometric functions cancel, making elementary the remaining angle integral. To this end we note the two relevant angle integrals:

$$\int_0^{2\pi} \frac{d\theta}{2\pi} m(\theta) = \sqrt{m_x m_y}$$

and

$$\int_0^{2\pi} \frac{d\theta}{2\pi} \cos^2(\theta)\, m^2(\theta) = \frac{1}{2}\sqrt{m_x m_y} m_x.$$

Then we obtain the final expression for the integral (A1),

$$n_i u_0^2 \int \frac{d\mathbf{p}}{(2\pi)^2} \mathcal{G}_{\mathbf{p}}^R \frac{p_x}{m_x} \mathcal{G}_{\mathbf{p}}^A = \alpha_x s_y, \tag{A2}$$

which is a remarkble result being dependent only on the Rashba anisotropy.

[1] S. Datta and B. Das, Electronic analog of the electro-optic modulator, Appl. Phys. Lett. **56**, 665 (1990).

[2] J. Nitta, T. Akazaki, H. Takayanagi, and T. Enoki, Gate control of spin-orbit interaction in an inverted $In_{0.53}Ga_{0.47}as/In_{0.52}Al_{0.48}as$ heterostructure, Phys. Rev. Lett. **78**, 1335 (1997).

[3] R. H. Silsbee, Spin–orbit induced coupling of charge current and spin polarization, J. Phys.: Condens. Matter **16**, R179 (2004).

[4] A. Hirohata and K. Takanashi, Future perspectives for spintronic devices, J. Phys. D **47**, 193001 (2014).

[5] S. D. Ganichev, M. Trushin, and J. Schliemann, Spin polarization by current, in *Handbook of Spin Transport and Magnetism*, edited by E. Y. Tsymbal and I. Zutic (Chapman and Hall, Boca Raton, FL, 2016), Chap. 24.

[6] A. Soumyanarayanan, N. Reyren, A. Fert, and C. Panagopoulos, Emergent phenomena induced by spin–orbit coupling at surfaces and interfaces, Nature (London) **539**, 509 (2016).

[7] G. Dresselhaus, Spin-orbit coupling effects in zinc blende structures, Phys. Rev. **100**, 580 (1955).

[8] E. I. Rashba, Properties of semiconductors with an extremum loop. 1. cyclotron and combinational resonance in a magnetic field perpendicular to the plane of the loop, Fiz. Tverd. Tela (Leningrad) **2**, 1224 (1960) [Sov. Phys. Solid State **2**, 1109 (1960)].

[9] E. L. Ivchenko and G. E. Pikus, New photogalvanic effect in gyrotropic crystals, Sov. J. Exp. Theor. Phys. Lett. **27**, 604 (1978).

[10] L. E. Vorob'ev, E. L. Ivchenko, G. E. Pikus, I. I. Farbshteĭn, V. A. Shalygin, and A. V. Shturbin, Optical activity in tellurium induced by a current, J. Exp. Theor. Phys. Lett. **29**, 441 (1979).

[11] C. L. Kane and E. J. Mele, Quantum spin Hall effect in graphene, Phys. Rev. Lett. **95**, 226801 (2005).

[12] M. I. D'yakonov, *Spin Physics in Semiconductor* (Springer, Berlin, 2008).

[13] D. Kochan, S. Irmer, and J. Fabian, Model spin-orbit coupling Hamiltonians for graphene systems, Phys. Rev. B **95**, 165415 (2017).

[14] T. P. Cysne, A. Ferreira, and T. G. Rappoport, Crystal-field effects in graphene with interface-induced spin-orbit coupling, Phys. Rev. B **98**, 045407 (2018).

[15] A. H. Castro Neto and F. Guinea, Impurity-induced spin-orbit coupling in graphene, Phys. Rev. Lett. **103**, 026804 (2009).

[16] C. Weeks, J. Hu, J. Alicea, M. Franz, and R. Wu, Engineering a robust quantum spin Hall state in graphene via Adatom deposition, Phys. Rev. X **1**, 021001 (2011).

[17] J. Balakrishnan, G. K. W. Koon, A. Avsar, Y. Ho, J. H. Lee, M. Jaiswal, S.-J. Baeck, J.-H. Ahn, A. Ferreira, M. A. Cazalilla, *et al.*, Giant spin Hall effect in graphene grown by chemical vapour deposition, Nat. Commun. **5**, 4748 (2014).

[18] I. Žutić, J. Fabian, and S. Das Sarma, Spintronics: Fundamentals and applications, Rev. Mod. Phys. **76**, 323 (2004).

[19] M. I. D'yakonov and V. I. Perel', Possibility of orienting electron spins with current, JETP Lett. **13**, 467 (1971).

[20] J. Sinova, D. Culcer, Q. Niu, N. A. Sinitsyn, T. Jungwirth, and A. H. MacDonald, Universal intrinsic spin Hall effect, Phys. Rev. Lett. **92**, 126603 (2004).

[21] S. Murakami, N. Nagaosa, and S.-C. Zhang, Dissipationless quantum spin current at room temperature, Science **301**, 1348 (2003).

[22] J. Sinova, S. O. Valenzuela, J. Wunderlich, C. H. Back, and T. Jungwirth, Spin Hall effects, Rev. Mod. Phys. **87**, 1213 (2015).

[23] D. T. S. Perkins, A. Veneri, and A. Ferreira, Spin Hall effect: Symmetry breaking, twisting, and giant disorder renormalization, Phys. Rev. B **109**, L241404 (2024).

[24] A. G. Aronov and Y. B. Lyanda-Geller, Nuclear electric resonance and orientation of carrier spins by an electric field, JETP Lett. **50**, 431 (1989) [Pisma Zh. Eksp. Teor. Fiz. **50**, 398 (1989)].

[25] E. L. Ivchenko, Y. B. Lyanda-Geller, and G. E. Pikus, Current of thermalized spin-oriented photocarriers, Sov. Phys. JETP **71**, 550 (1991) [Zh. Eksp. Teor. Fiz. **98**, 989 (1990)].

[26] S. D. Ganichev, E. L. Ivchenko, V. V. Belkov, S. A. Tarasenko, M. Sollinger, D. Weiss, W. Wegscheider, and W. Prettl, Spin-galvanic effect, Nature (London) **417**, 153 (2002).

[27] K. Shen, G. Vignale, and R. Raimondi, Microscopic theory of the inverse Edelstein effect, Phys. Rev. Lett. **112**, 096601 (2014).

[28] C. Gorini, A. Maleki Sheikhabadi, K. Shen, I. V. Tokatly, G. Vignale, and R. Raimondi, Theory of current-induced spin polarization in an electron gas, Phys. Rev. B **95**, 205424 (2017).

[29] M. Offidani, M. Milletarì, R. Raimondi, and A. Ferreira, Optimal charge-to-spin conversion in graphene on transition-metal dichalcogenides, Phys. Rev. Lett. **119**, 196801 (2017).

[30] A. Veneri, D. T. S. Perkins, and A. Ferreira, Nonperturbative approach to interfacial spin-orbit torques induced by the Rashba effect, Phys. Rev. B **106**, 235419 (2022).

[31] H.-A. Engel, B. I. Halperin, and E. I. Rashba, Theory of spin Hall conductivity in n-doped GaAs, Phys. Rev. Lett. **95**, 166605 (2005).

[32] W.-K. Tse and S. Das Sarma, Spin Hall effect in doped semiconductor structures, Phys. Rev. Lett. **96**, 056601 (2006).

[33] E. M. Hankiewicz and G. Vignale, Phase diagram of the spin Hall effect, Phys. Rev. Lett. **100**, 026602 (2008).

[34] R. Raimondi and P. Schwab, Tuning the spin Hall effect in a two-dimensional electron gas, Europhys. Lett. **87**, 37008 (2009).

[35] R. Raimondi, P. Schwab, C. Gorini, and G. Vignale, Spin-orbit interaction in a two-dimensional electron gas: A $SU(2)$ formulation, Ann. Phys. **524**, 201100253 (2012).

[36] M. Milletarì and A. Ferreira, Quantum diagrammatic theory of the extrinsic spin Hall effect in graphene, Phys. Rev. B **94**, 134202 (2016).

[37] C. L. Kane and E. J. Mele, Z_2 topological order and the quantum spin Hall effect, Phys. Rev. Lett. **95**, 146802 (2005).

[38] C. Huang, Y. D. Chong, and M. A. Cazalilla, Direct coupling between charge current and spin polarization by extrinsic mechanisms in graphene, Phys. Rev. B **94**, 085414 (2016).

[39] Y. A. Bychkov and É. I. Rashba, Properties of a 2d electron gas with lifted spectral degeneracy, JETP Lett. **39**, 78 (1984).

[40] Y. K. Kato, R. C. Myers, A. C. Gossard, and D. D. Awschalom, Current-induced spin polarization in strained semiconductors, Phys. Rev. Lett. **93**, 176601 (2004).

[41] V. Sih, R. C. Myers, Y. K. Kato, W. H. Lau, A. C. Gossard, and D. D. Awschalom, Spatial imaging of the spin Hall effect and current-induced polarization in two-dimensional electron gases, Nat. Phys. **1**, 31 (2005).

[42] J. C. R. Sánchez, L. Vila, G. Desfonds, S. Gambarelli, J. P. Attané, J. M. De Teresa, C. Magén, and A. Fert, Spin-to-charge conversion using Rashba coupling at the interface between non-magnetic materials, Nat. Commun. **4**, 2944 (2013).

[43] E. Lesne, S. O. Yu Fu, J. C. Rojas-Sánchez, D. C. Vaz, H. Naganuma, G. Sicoli, J.-P. Attané, M. Jamet, E. Jacquet, J.-M. George, A. Barthélémy, H. Jaffrès, A. Fert, M. Bibes, and L. Vila, Highly efficient and tunable spin-to-charge conversion through Rashba coupling at oxide interfaces, Nat. Mater. **15**, 1261 (2016).

[44] Y. Shiomi, K. Nomura, Y. Kajiwara, K. Eto, M. Novak, K. Segawa, Y. Ando, and E. Saitoh, Spin-Electricity Conversion Induced by Spin Injection into Topological Insulators, Phys. Rev. Lett. **113**, 196601 (2014).

[45] A. R. Mellnik, J. S. Lee, A. Richardella, J. L. Grab, P. J. Mintun, M. H. Fischer, A. Vaezi, A. Manchon, E.-A. Kim, N. Samarth, and D. C. Ralph, Spin-transfer torque generated by a topological insulator, Nature (London) **511**, 449 (2014).

[46] A. A. Burkov, A. S. Núñez, and A. H. MacDonald, Theory of spin-charge-coupled transport in a two-dimensional electron gas with Rashba spin-orbit interactions, Phys. Rev. B **70**, 155308 (2004).

[47] C. Gorini, P. Schwab, R. Raimondi, and A. L. Shelankov, Non-abelian gauge fields in the gradient expansion: Generalized Boltzmann and Eilenberger equations, Phys. Rev. B **82**, 195316 (2010).

[48] C. Gorini, R. Raimondi, and P. Schwab, Onsager relations in a two-dimensional electron gas with spin-orbit coupling, Phys. Rev. Lett. **109**, 246604 (2012).

[49] A. A. Burkov and D. G. Hawthorn, Spin and charge transport on the surface of a topological insulator, Phys. Rev. Lett. **105**, 066802 (2010).

[50] A. Ferreira, Theory of spin–charge-coupled transport in proximitized graphene: An SO(5) algebraic approach, J. Phys.: Mater. **4**, 045006 (2021).

[51] A. Veneri, D. T. S. Perkins, C. G. Péterfalvi, and A. Ferreira, Twist angle controlled collinear Edelstein effect in van der Waals heterostructures, Phys. Rev. B **106**, L081406 (2022).

[52] E. Simon, A. Szilva, B. Ujfalussy, B. Lazarovits, G. Zarand, and L. Szunyogh, Anisotropic Rashba splitting of surface states from the admixture of bulk states: Relativistic *ab initio* calculations and $k \cdot p$ perturbation theory, Phys. Rev. B **81**, 235438 (2010).

[53] S. Chakraborty and S. Raj, Tunable nonlinear anisotropic Rashba splitting in monolayer transition metal dichalcogenide $MoS_{2(1-x)}Se_{2x}$ alloys, Phys. Rev. B **108**, 165402 (2023).

[54] B. Geldiyev, M. Ünzelmann, P. Eck, T. Kißlinger, J. Schusser, T. Figgemeier, P. Kagerer, N. Tezak, M. Krivenkov, A. Varykhalov, A. Fedorov, L. Nicolaï, J. Minár, K. Miyamoto, T. Okuda, K. Shimada, D. Di Sante, G. Sangiovanni, L. Hammer, M. A. Schneider, *et al.*, Strongly anisotropic spin and orbital rashba effect at a tellurium–noble metal interface, Phys. Rev. B **108**, L121107 (2023).

[55] D. V. Gruznev, L. V. Bondarenko, A. Y. Tupchaya, V. G. Kotlyar, O. A. Utas, A. N. Mihalyuk, S. V. Eremeev, A. V. Zotov, and A. A. Saranin, Two-dimensional metallic (Tl, Au)/Si(100)$c(2 \times 2)$: A Rashba-type system with C_{2v} symmetry, Phys. Rev. B **98**, 125428 (2018).

[56] L. Fu, Hexagonal warping effects in the surface states of the topological insulator Bi_2Te_3, Phys. Rev. Lett. **103**, 266801 (2009).

[57] E. Frantzeskakis and M. Grioni, Anisotropy effects on Rashba and topological insulator spin-polarized surface states: A unified phenomenological description, Phys. Rev. B **84**, 155453 (2011).

[58] K. Miyamoto, H. Miyahara, K. Kuroda, T. Maegawa, A. Kimura, and T. Okuda, Peculiar Rashba spin texture induced by C_{3v} symmetry on the Bi(111) surface revisited, Phys. Rev. B **97**, 085433 (2018).

[59] J. Ibañez-Azpiroz, A. Bergara, E. Y. Sherman, and A. Eiguren, Spin-flip transitions and departure from the Rashba model in the Au(111) surface, Phys. Rev. B **88**, 125404 (2013).

[60] E. E. Krasovskii, Microscopic origin of the relativistic splitting of surface states, Phys. Rev. B **90**, 115434 (2014).

[61] A. Johansson, J. Henk, and I. Mertig, Theoretical aspects of the Edelstein effect for anisotropic two-dimensional electron gas and topological insulators, Phys. Rev. B **93**, 195440 (2016).

[62] I. Miatka, M. Barbieri, and R. Raimondi, Nonlinear inverse spin galvanic effect in anisotropic disorder-free systems, Eur. Phys. J. D **73**, 107 (2019).

[63] S. Leiva-Montecinos, J. Henk, I. Mertig, and A. Johansson, Spin and orbital Edelstein effect in a bilayer system with Rashba interaction, Phys. Rev. Res. **5**, 043294 (2023).

[64] I. Gaiardoni, M. Trama, A. Maiellaro, C. Guarcello, F. Romeo, and R. Citro, Edelstein effect in isotropic and anisotropic Rashba models, Condens. Matter **10**, 15 (2025).

[65] G. Grosso and G. Parravicini, *Solid State Physics* (Academic Press, New York, 2000).

[66] J. Ziman, *Electrons and Phonons: The Theory of Transport Phenomena in Solids*, International Series of Monographs on Physics (Oxford University Press, Oxford, 2001).

[67] E. G. Mishchenko, A. V. Shytov, and B. I. Halperin, Spin current and polarization in impure two-dimensional electron systems with spin-orbit coupling, Phys. Rev. Lett. **93**, 226602 (2004).

[68] A. Khaetskii, Intrinsic spin current for an arbitrary Hamiltonian and scattering potential, Phys. Rev. B **73**, 115323 (2006).

[69] C. Xiao and Q. Niu, Semiclassical theory of spin-orbit torques in disordered multiband electron systems, Phys. Rev. B **96**, 045428 (2017).

[70] A. Sekine, D. Culcer, and A. H. MacDonald, Quantum kinetic theory of the chiral anomaly, Phys. Rev. B **96**, 235134 (2017).

[71] R. Kubo, A general expression for the conductivity tensor, Can. J. Phys. **34**, 1274 (1956).

[72] R. Kubo, Statistical-mechanical theory of irreversible processes. I. general theory and simple applications to magnetic and conduction problems, J. Phys. Soc. Jpn. **12**, 570 (1957).

[73] A. Bastin, C. Lewiner, O. Betbeder-matibet, and P. Nozieres, Quantum oscillations of the Hall effect of a fermion gas with random impurity scattering, J. Phys. Chem. Solids **32**, 1811 (1971).

[74] P. Středa and L. Smrčka, Galvanomagnetic effects in alloys in quantizing magnetic fields, Phys. Status Solidi B **70**, 537 (1975).

[75] D. Xiao, M.-C. Chang, and Q. Niu, Berry phase effects on electronic properties, Rev. Mod. Phys. **82**, 1959 (2010).

[76] I. A. Ado, I. A. Dmitriev, P. M. Ostrovsky, and M. Titov, Anomalous Hall effect with massive Dirac fermions, Europhys. Lett. **111**, 37004 (2015).

[77] I. A. Ado, O. A. Tretiakov, and M. Titov, Microscopic theory of spin-orbit torques in two dimensions, Phys. Rev. B **95**, 094401 (2017).

[78] N. A. Sinitsyn, A. H. MacDonald, T. Jungwirth, V. K. Dugaev, and J. Sinova, Anomalous Hall effect in a two-dimensional Dirac band: The link between the Kubo-streda formula and the semiclassical Boltzmann equation approach, Phys. Rev. B **75**, 045315 (2007).

[79] T. Valet and R. Raimondi, Quantum kinetic theory of the linear response for weakly disordered multiband systems, Phys. Rev. B **111**, L041118 (2025).

[80] D. Go, H.-W. Lee, P. M. Oppeneer, S. Blügel, and Y. Mokrousov, First-principles calculation of orbital Hall effect by Wannier interpolation: Role of orbital dependence of the anomalous position, Phys. Rev. B **109**, 174435 (2024).

[81] D. García Ovalle, A. Pezo, and A. Manchon, Spin-orbit torque for field-free switching in C_{3v} crystals, Phys. Rev. B **107**, 094422 (2023).

[82] R. Raimondi and P. Schwab, Spin-Hall effect in a disordered two-dimensional electron system, Phys. Rev. B **71**, 033311 (2005).

[83] J.-i. Inoue, G. E. W. Bauer, and L. W. Molenkamp, Suppression of the persistent spin Hall current by defect scattering, Phys. Rev. B **70**, 041303 (2004).

[84] O. V. Dimitrova, Spin-Hall conductivity in a two-dimensional Rashba electron gas, Phys. Rev. B **71**, 245327 (2005).

[85] O. Chalaev and D. Loss, Spin-Hall conductivity due to Rashba spin-orbit interaction in disordered systems, Phys. Rev. B **71**, 245318 (2005).

[86] V. Bonbien and A. Manchon, Symmetrized decomposition of the Kubo-Bastin formula, Phys. Rev. B **102**, 085113 (2020).

[87] L. Smrcka and P. Streda, Transport coefficients in strong magnetic fields, J. Phys. C **10**, 2153 (1977).

[88] A. Crépieux and P. Bruno, Theory of the anomalous Hall effect from the Kubo formula and the Dirac equation, Phys. Rev. B **64**, 014416 (2001).

[89] C. Di Castro and R. Raimondi, *Statistical Mechanics and Applications in Condensed Matter* (Cambridge University Press, Cambridge, 2015).

[90] A. Kamenev, *Field Theory of Non-Equilibrium Systems* (Cambridge University Press, Cambridge, 2011).

[91] R. Raimondi, M. Leadbeater, P. Schwab, E. Caroti, and C. Castellani, Spin-orbit induced anisotropy in the magnetoconductance of two-dimensional metals, Phys. Rev. B **64**, 235110 (2001).

[92] R. Raimondi and P. Schwab, Magnetoconductance of a two-dimensional metal in the presence of spin-orbit coupling, Eur. Phys. J. B **25**, 483 (2002).

[93] M. Offidani, R. Raimondi, and A. Ferreira, Microscopic linear response theory of spin relaxation and relativistic transport phenomena in graphene, Condens. Matter **3**, 18 (2018).

[94] T. Valet and R. Raimondi, Semiclassical kinetic theory for systems with non-trivial quantum geometry and the expectation value of physical quantities, Europhys. Lett. **143**, 26004 (2023).

[95] L. V. Keldysh, Diagram Technique for Nonequilibrium Processes, Sov. Phys. JETP **20**, 1018 (1965).

[96] A. Larkin and Y. Ovchinnikov, Nonlinear conductivity of superconductors in the mixed state, Sov. Phys. JETP **41**, 960 (1975).

[97] T. Valet, H. Jaffres, V. Cros, and R. Raimondi, Quantum kinetic anatomy of electron angular momenta edge accumulation, Phys. Rev. Lett. **135**, 256301 (2025).

[98] R. Raimondi and T. Valet, Quantum kinetic theory of the spin Hall effect for disordered graphene with Rashba spin–orbit coupling, Condens. Matter **10**, 4 (2025).

[99] A. Veneri, P. Burghignoli, and D. Comite, Microwave imaging with circular arrays: Comparative analysis between OAM and MIMO, IEEE Trans. Antennas Propag. **73**, 3015 (2025).

[100] J. Rammer, *Quantum Transport Theory* (CRC Press, Boca Raton, FL, 2018).

[101] M. Milletarì, M. Offidani, A. Ferreira, and R. Raimondi, Covariant conservation laws and the spin Hall effect in Dirac-Rashba systems, Phys. Rev. Lett. **119**, 246801 (2017).

[102] B. M. Norman, C. J. Trowbridge, D. D. Awschalom, and V. Sih, Current-induced spin polarization in anisotropic spin-orbit fields, Phys. Rev. Lett. **112**, 056601 (2014).